



**Environmental
Science**
Processes & Impacts

**Photodecay of guaiacol is faster in ice, and even more rapid
on ice, than in aqueous solution**

Journal:	<i>Environmental Science: Processes & Impacts</i>
Manuscript ID	EM-ART-05-2020-000242.R1
Article Type:	Paper

SCHOLARONE™
Manuscripts

1
2
3 Snow has long been recognized as an important part of our environment, providing benefits
4 ranging from transportation to drinking water. More recently, research has revealed snow to be a
5 particularly important site for photochemical reactions, for reasons including deep penetration of
6 light into the snowpack and long summer days in polar regions. However, there is considerable
7 debate over the speed of these reactions, with some research showing faster photodegradation of
8 chemicals on snow or ice versus in aqueous solution. Using guaiacol as a model compound, we
9 find reaction rates at the snow surface considerably faster than in solution, primarily due to
10 increased quantum yield. These results indicate some chemicals in/on snow degrade faster than
11 previously known, reducing their environmental lifetimes.
12
13
14
15
16
17
18
19
20
21
22
23
24
25
26
27
28
29
30
31
32
33
34
35
36
37
38
39
40
41
42
43
44
45
46
47
48
49
50
51
52
53
54
55
56
57
58
59
60

1 Photodecay of guaiacol is faster in ice, and even more rapid on ice, than in aqueous solution

2 Ted Hullar¹, Fernanda Bononi², Zekun Chen², Danielle Magadia^{1,3}, Oliver Palmer^{1,4}, Theo
3 Tran¹, Dario Rocca⁵, Oliviero Andreussi⁶, Davide Donadio², and Cort Anastasio^{1,*}

4 ¹ Department of Land, Air and Water Resources, University of California, Davis, One
5 Shields Avenue, Davis, CA 95616, USA

6 ² Department of Chemistry, University of California, Davis, One Shields Avenue, Davis,
7 CA 95616, USA

8 ³ Now at California Air Resources Board, 1001 I Street, Sacramento, CA 95814

9 ⁴ Now at TeraPore Technologies, 407 Cabot Road, South San Francisco, CA 94080

10 ⁵ Université de Lorraine, CNRS, LPCT, F-54000 Nancy, France

11 ⁶ Department of Physics, University of North Texas, 1155 Union Circle, #311427, Denton,
12 Texas 76203.

13 * Corresponding author, canastasio@ucdavis.edu, (530) 754-6095

15 Environmental Significance Statement

16 Snow has long been recognized as an important part of our environment, providing benefits
17 ranging from transportation to drinking water. More recently, research has revealed snow to be a
18 particularly important site for photochemical reactions, for reasons including deep penetration of
19 light into the snowpack and long summer days in polar regions. However, there is considerable
20 debate over the speed of these reactions, with some research showing faster photodegradation of
21 chemicals on snow or ice versus in aqueous solution. Using guaiacol as a model compound, we
22 find reaction rates at the snow surface considerably faster than in solution, primarily due to
23 increased quantum yield. These results indicate some chemicals in/on snow degrade faster than
24 previously known, reducing their environmental lifetimes.

26 Abstract

27 Snowpacks contain a wide variety of inorganic and organic compounds, including some that
28 absorb sunlight and undergo direct photoreactions. How the rates of these reactions in, and on,
29 ice compare to rates in water is unclear: some studies report similar rates, while others find faster
30 rates in/on ice. Further complicating our understanding, there is conflicting evidence whether
31 chemicals react more quickly at the air-ice interface compared to in liquid-like regions (LLRs)
32 within the ice. To address these questions, we measured the photodegradation rate of guaiacol
33 (2-methoxyphenol) in various sample types, including in solution, in ice, and at the air-ice
34 interface of nature-identical snow. Compared to aqueous solution, we find modest rate constant
35 enhancements (increases of 3- to 6-fold) in ice LLRs, and much larger enhancements (of 17- to

77-fold) at the air-ice interface of nature-identical snow. Our computational modeling suggests the absorption spectrum for guaiacol red-shifts and increases on ice surfaces, leading to more light absorption, but these changes explain only a small portion (roughly 2 to 9%) of the observed rate constant enhancements in/on ice. This indicates that increases in the quantum yield are primarily responsible for the increased photoreactivity of guaiacol on ice; relative to solution, our results suggest that the quantum yield is larger by a factor of roughly 3-6 in liquid-like regions and 12-40 at the air-ice interface.

1.0 Introduction

Snow is an active location for chemical reactions,^{1,2} which can release pollutants to the atmosphere, act as sinks for toxic species, and alter the concentrations of markers used in ice core research to understand past atmospheres.³ For example, photochemical reactions of organic compounds – some of which are toxic – transform the pollutants into more volatile molecules, such as formaldehyde, that can be released to the atmosphere.^{4,5}

Deposited snow and ice are primarily composed of crystalline water ice, but also contain small areas of disordered water molecules where most solutes reside.^{1,3,6,7} These disordered regions exist both at the air-ice interface (which is also referred to as the quasi-liquid layer (QLL) or disordered interface) and within liquid-like regions (LLRs) in the ice matrix (e.g., at grain boundaries). Much of snowpack chemistry appears to be driven by light,³ in part because sunlight can reach tens of centimeters into the snowpack.⁸⁻¹⁰ Compounds that absorb sunlight can undergo direct photoreactions, i.e., chemical transformations as a result of the absorbed energy.

Despite their importance, the rates of relatively few direct photochemical reactions in snow and ice have been quantified. Further confounding our understanding, past results give conflicting pictures of reaction rates for molecules in/on ice, with some work showing rate enhancements in/on ice compared to solution and other work showing no enhancement. Early work by Kahan and Donaldson¹¹ found that rates of photodegradation for toxic polycyclic aromatic hydrocarbons (PAHs) were enhanced on ice compared to in aqueous solution. For example, anthracene and naphthalene photodegradations were approximately six and nine times faster, respectively, at the air-ice interface. Later work from the same group¹² found a four-fold rate enhancement for anthracene at the interface and only a 1.6-fold enhancement in LLRs. Photodegradation of the aromatic compound harmine at the air-ice interface was enhanced by a factor of 4 compared to solution, but was not measured in LLRs.¹³

In contrast to these studies showing rate enhancements in/on ice, other work has found that photodegradation is not enhanced in ice relative to solution. For example, direct photodegradation of a number of inorganic solutes, including nitrate, nitrite, and hydrogen peroxide, is described by the same temperature-dependent relationship in LLRs and in aqueous solution.¹⁴⁻¹⁶ In addition, similar rates in solution and ice LLRs have been reported for phenanthrene, pyrene, and fluoranthene.¹⁷ Similarly, we found that anthracene and pyrene each had similar photodegradation rates in solution, in ice LLRs, and at the air-ice interface.¹⁸

The rate of photodecay for chemical “C” ($M s^{-1}$) in a low-light absorbing medium (e.g., solution or ice) during sunlight illumination is:¹⁶

78

79

$$\frac{d[C]}{dt} = - \sum_{\lambda} \frac{2303}{N_A} I_{\lambda} \Delta\lambda \Phi_{C, \lambda} \varepsilon_{C, \lambda} [C] \quad (1)$$

80

81 where 2303 is a factor for units and base conversion ($1000 \text{ cm}^3 \text{ L}^{-1}$), N_A is Avogadro's number
 82 ($6.022 \times 10^{23} \text{ molecules mol}^{-1}$), I_{λ} is the actinic flux at each wavelength ($\text{photons cm}^{-2} \text{ s}^{-1} \text{ nm}^{-1}$),
 83 $\Delta\lambda$ is the wavelength interval between photon flux data points (nm), $\varepsilon_{C, \lambda}$ is the wavelength-
 84 dependent molar absorptivity for C ($\text{M}^{-1} \text{ cm}^{-1}$), $\Phi_{C, \lambda}$ is the quantum yield for loss of C (molecule
 85 photon^{-1}), and $[C]$ is the concentration. Based on equation 1, three factors could enhance
 86 reaction rates in/on ice relative to solution: higher local photon fluxes, higher quantum yields,
 87 and/or a bathochromic shift (i.e., to longer wavelengths) in molar absorptivity, which shifts light
 88 absorption to regions with more photons.

89

90 Most previous work did not measure photon fluxes, making it difficult to fully assess whether the
 91 photon flux might have been higher in/on ice compared to solution. While the photon flux in
 92 near-surface snow can be up to twice as high as in the overlying air,^{8,19,20} enhancements in
 93 laboratory ices are smaller.²¹ Thus, differences in photon fluxes between ice and solution do not
 94 appear to be able to explain the observed ice enhancements in past work.

95 The second possibility is an enhancement in the quantum yield for loss, i.e., the fraction of
 96 absorbed photons that results in loss of C. Quantum yields for PAHs are similar in LLRs and
 97 solution,¹⁷ while quantum yields for nitrate, nitrite, and hydrogen peroxide in LLRs follow the
 98 same temperature dependence as in aqueous solution, suggesting similar reaction
 99 environments.¹⁴⁻¹⁶ However, Zhu and coworkers²² reported a quantum yield for nitrate
 100 photolysis at the air-ice interface that is over 200 times higher than found by Chu and
 101 Anastasio¹⁶ for nitrate in LLRs. Further, McFall et al.²³ recently found that nitrate photolysis is
 102 more efficient at the air-ice interface compared to in LLRs, but only by a factor of ~ 3 .
 103 However, even at this lower enhancement, a higher quantum yield could explain a significant
 104 portion of the reported reaction rate increases for PAHs at the air-ice interface.

105 The third possible reason for an enhancement in rates of direct photodegradation in/on ice is that
 106 the molar absorptivities are shifted to the red (i.e., bathochromically). Because the abundance of
 107 solar photons increases dramatically at longer wavelengths between 290 and 400 nm, even a
 108 small bathochromic shift of absorbance in/on ice could significantly increase the rate of sunlight
 109 absorption and thus the reaction rate. Several studies have examined this possibility by
 110 measuring absorbance in LLRs and/or at the air-ice interface for a variety of chemicals.²⁴⁻³⁰ For
 111 phenols and naphthalene, absorbance in/on ice is the same as in aqueous solution,^{26,28} while
 112 anisole exhibits a small 4-nm bathochromic (red) shift in both LLRs and QLLs relative to
 113 solution.²⁹ Three aniline derivatives show a substantial 10-15 nm red shift in both LLRs and
 114 QLLs.³⁰ In contrast, methylene blue, nitrate, and nitrite in LLRs exhibit hypsochromic (blue)
 115 shifts of approximately, 10, 1, and 2 nm, respectively.²⁷ However, measuring absorbance at the
 116 air-ice interface can be problematic because it requires a relatively high concentration of
 117 molecules, which tends to lead to self-association, possibly changing absorption relative to what
 118 occurs for the much lower concentrations in natural snow.

119 Because of the difficulties in experimentally measuring light absorbance of molecules at the air-
 120 ice interface, a number of groups have instead relied upon molecular modeling.³¹⁻³⁴ In

1
2
3 121 particular, quantum chemical (QC) calculations have been used to interpret spectroscopic
4 122 measurements of UV-Vis absorption and emission for organic compounds present in LLRs or at
5 123 the air-ice interface.^{25,28,29,35} However, the modeling approach used in these former works
6 124 cannot directly predict shifts in the UV-visible spectra due to different solvation environments.

7
8 125 Previous experimental work done with solutes on ice surfaces, in our laboratory and others, have
9 126 attempted to reproduce the physical reaction environment of snow by a variety of methods,
10 127 including freezing aqueous solution in molds, spraying aqueous solutions into liquid nitrogen to
11 128 form ice pellets, or grinding solute-containing ices into small pieces.^{8,12,15,16,36,37} However, snow
12 129 crystals are quite complex, and none of these past methods for making impurity-containing snow
13 130 analogs accurately mimic the complex structure and measured physical properties of newly-
14 131 fallen natural snow crystals. For example, new natural snow has a specific surface area (SSA, the
15 132 ratio of sample surface area to ice mass) of approximately 1,000 cm² g⁻¹.³⁸ However, a frozen
16 133 water sample in a beaker can have an SSA of <1 cm² g⁻¹, increasing the likelihood that a test
17 134 compound vapor deposited to that ice surface will aggregate.

18
19
20 135 To address the relative importance of changes in quantum yield and/or absorbance in ice
21 136 compared to solution, here we measure the photodegradation rate constant of a model organic
22 137 compound, guaiacol, which is emitted from biomass burning.³⁹ We study guaiacol (GUA)
23 138 photodecay in several experimental preparations, including in solution, in ice, and at the air-ice
24 139 interface on nature-identical snow crystals. In each case we measure photon fluxes to account
25 140 for this variable. We also use a multiscale approach,⁴⁰ based on molecular dynamics (MD),
26 141 quantum-mechanical calculations and statistical learning, to model the absorbance of guaiacol in
27 142 aqueous solution and on an ice surface. We have two main goals: 1) to examine whether direct
28 143 photodegradation of guaiacol is enhanced (relative to solution) in LLRs or at the air-ice interface
29 144 of nature-identical snow, and 2) to understand the mechanism(s) for any enhancements.

30 145 **2 Methods**

31 146 **2.1 Materials**

32
33
34
35 147 Guaiacol (98%) was from Sigma or TCI. Acetonitrile (HPLC grade) was from Acros. 2-
36 148 nitrobenzaldehyde (2NB, 98%) was from Sigma-Aldrich. High purity water (MQ) was from
37 149 house-treated R/O water that was run through a Barnstead International DO813 activated carbon
38 150 cartridge and then a Millipore Milli-Q system (≥ 18.2 M Ω cm).

39 151 **2.2 Sample preparation**

40
41
42
43 152 Most samples were illuminated in either a 5-ml glass beaker (made by cutting the threads and
44 153 neck off a 7-ml glass vial) or 10-ml glass beaker (Pyrex). Samples were covered with
45 154 polyethylene film (ClingWrap brand, Glad Products Company, approximately 8 μ m thick), held
46 155 in place with an o-ring, to control guaiacol evaporation and sample contamination.

47
48
49 156
50 157 Samples were prepared with one of five different methods (Supplementary Figure S1): 1)
51 158 Aqueous solution, where guaiacol was dissolved in MQ water to give a final concentration of 1.0
52 159 μ M, then either 5 or 10 ml of solution was placed in a beaker and covered. 2) Freezer frozen
53 160 solution, where 5 or 10 ml of a 1.0 μ M aqueous solution was placed in a beaker, covered, and
54 161 frozen in a laboratory freezer at -20 °C over approximately 3 hours. 3) Liquid nitrogen frozen
55 162 solution, where samples were prepared from aqueous solution, put into a beaker, then placed in a
56
57
58
59
60

1
2
3 163 pan filled with liquid nitrogen to a depth of approximately 2 cm. Freezing took approximately
4 164 90 seconds. 4) Vapor deposition of gas-phase guaiacol to the top surface of frozen water ice; our
5 165 method here follows the same approach as previously described.¹⁸ First, 10 ml of MQ water was
6 166 placed in a beaker, covered with PE film, and frozen in a laboratory freezer at -20 °C. Once
7 167 frozen, samples were removed and uncovered, and a nitrogen stream containing gas-phase
8 168 guaiacol was directed at the ice surface for 15 s. Samples were then covered and placed back in
9 169 a laboratory freezer. 5) Vapor deposited to nature-identical snow.
10 170

11
12 171 For this last method, we first made nature-identical snow crystals, using a custom-built machine
13 172 based on previous work,^{38,41,42} described in Supplementary Section S3 and shown in Figure S2.
14 173 This device, which is placed in a cold room at approximately -15 °C, uses the principle of
15 174 nucleating supersaturated water vapor to form snow crystals (Figures S3 and S4, and
16 175 Supplemental Movie M1). To treat the snow with guaiacol, nitrogen from a tank in the cold
17 176 room was directed first through a HDPE wide-mouth bottle (500 or 1000 ml) holding laboratory-
18 177 made snow to introduce water vapor. The gas was then passed through a glass container holding
19 178 0.4 g of guaiacol solid and then through another 500- or 1000-ml HDPE bottle holding snow to
20 179 be treated, where guaiacol was deposited to the snow. Supplementary Figure S1b shows the
21 180 treatment system. The treated snow was then gently mixed using two stainless steel spoons and
22 181 transferred to individual 5- or 10-ml beakers for subsequent illumination. In the case of the LC2
23 182 condition (described below), the snow was tamped down 10 mm with a plastic plug before
24 183 covering so that the snow level was no higher than the level of the cooled aluminum block in the
25 184 illumination system. We noticed some subsidence in the snow level, particularly at the center of
26 185 the beaker for 24-hour or longer experiments, probably attributable to metamorphism in the snow
27 186 crystals. However, the overall appearance of the snow did not change, and there was no
28 187 evidence of melting.
29
30
31
32

33 189 **2.3 Sample illumination, actinometry, and chemical analysis**

34
35 190 Sample illumination generally followed the method described for anthracene and pyrene.¹⁸
36 191 Sample beakers were set upright in a drilled aluminum holder to maximize heat transfer and
37 192 minimize the impact of sample heating from the illumination source. Dark samples were
38 193 covered with aluminum foil and placed in the illumination chamber along with illuminated
39 194 samples. Sample temperatures were held at 5 (for aqueous) or -10 °C (for ice and snow). For all
40 195 experiments, the light source was a filtered 1000 W Xenon arc lamp. The first set of
41 196 experiments was done using an AM1.5 airmass filter (Sciencetech), intended to filter the lamp
42 197 source to approximate solar sunlight. We identify these experiments as Light Condition 1
43 198 (“LC1”). However, we later determined this filter significantly transmits light between 250 and
44 199 290 nm, which does not exist in tropospheric sunlight. Therefore, we ran additional experiments
45 200 with three optical filters to better simulate sunlight: the airmass filter, a 295 longpass filter to
46 201 eliminate shorter wavelengths transmitted by the airmass filter, and a 400 shortpass filter (both
47 202 from Andover Corporation) to eliminate longer wavelengths that contribute to sample heating;
48 203 we refer to these experiments as being conducted under Light Condition 2 (“LC2”).
49
50
51

52 204 After illumination, we melted the frozen samples and measured guaiacol concentrations using a
53 205 Shimadzu HPLC¹⁸ with an eluent of 60:40 acetonitrile:MQ water, a flow rate of 0.700 ml min⁻¹,
54 206 and a detection wavelength of 276 nm. Frozen samples were melted (still covered with PE) and
55 207 then transferred to HPLC autosampler vials for analysis.
56
57
58
59
60

208 We used 2-nitrobenzaldehyde (2NB) as a chemical actinometer to normalize for differing photon
 209 fluxes across sample types and experimental days.^{18,20} With the exception of snow samples, on
 210 each experiment day we prepared actinometry samples with 10 μM 2NB using the same sample
 211 preparation and experimental treatment as in the parallel guaiacol illuminations, and illuminated
 212 the 2NB samples to measure $j_{2\text{NB}}$.¹⁸ Because measuring $j_{2\text{NB}}$ in snow on each experimental day
 213 was not practical, we measured $j_{2\text{NB}}$ in snow and in aqueous solution on three different days, then
 214 calculated the ratio of snow to aqueous measurements. For subsequent guaiacol
 215 photodegradation experiments in snow, we used this ratio (0.38 ± 0.015 (1 SD) for 10-ml
 216 beakers, 0.36 ± 0.13 for 5-ml beakers) along with the measured aqueous $j_{2\text{NB}}$ on that day to
 217 estimate the snow $j_{2\text{NB}}$.

218 2.4 Determining rate constants and quantum yields for guaiacol loss

219 To determine guaiacol photodegradation rate constants we followed the same approach used by
 220 Hullar et al.¹⁸ for PAHs. We illuminated samples, and periodically removed them from the
 221 illumination system and analyzed for guaiacol (section 2.3). For each experiment, we
 222 determined the photodegradation rate constant by first taking the natural logarithm of the ratio of
 223 each measured guaiacol concentration at time t to the initial guaiacol concentration, then
 224 adjusting these ratios by the photon-flux correction factor for each sample position.¹⁸ The slope
 225 of these points gives the pseudo-first-order rate constant for loss during illumination, j_{GUA} .
 226 Similar treatment of the dark controls gives the rate constant for dark loss, $k'_{\text{GUA,dark}}$; subtracting
 227 the dark rate constant from j_{GUA} gives the dark-corrected photodegradation rate constant, $j_{\text{GUA,exp}}$.
 228 Finally, to normalize for the experimental photon flux, we divided $j_{\text{GUA,exp}}$ by the daily measured
 229 $j_{2\text{NB}}$ value to give the photon flux-normalized j^*_{GUA} .

230 To calculate the average quantum yield for guaiacol (Φ_{GUA}) we used our previously determined
 231 $j_{\text{GUA,exp}}$, which can be expressed as:

$$232 \quad j_{\text{GUA,exp}} = \frac{2303}{N_A} \Phi_{\text{GUA}} \sum_{\lambda} (\epsilon_{\text{GUA},\lambda} I_{\lambda} \Delta\lambda) \quad (2)$$

233 and solved this equation for Φ_{GUA} . We determined molar absorptivities for guaiacol ($\epsilon_{\text{GUA},\lambda}$) by
 234 measuring absorbance spectra in five aqueous guaiacol solutions (10-1000 μM) at 25 $^{\circ}\text{C}$ using a
 235 UV-2501PC spectrophotometer (Shimadzu) in 1.0 cm cuvettes against a MQ reference cell. For
 236 each wavelength, we calculated the base-10 molar absorptivity as the slope of the linear
 237 regression of measured absorbance (divided by the 1-cm pathlength) versus the guaiacol
 238 concentration. As described in Supplementary Section S1, we determined I_{λ} by measuring $j_{2\text{NB}}$
 239 and relative photon fluxes at a reference position for each light condition. The quantum yield
 240 determined using equation 2 represents an average value over the guaiacol absorbance range of
 241 250 to the end of absorption, approximately 317 nm.

242 2.5 Computational methods

243 We use a combination of classical and first-principles molecular dynamics (FPMD) simulations,
 244 excited state calculations by time-dependent density functional theory (TDDFT), and machine
 245 learning to determine UV-visible absorption bands at finite temperature, including the effects of
 246 both long-range and local dielectric screening. We performed first-principles MD simulations of
 247 guaiacol in solution at 27 $^{\circ}\text{C}$ and the air-ice interface at -10 $^{\circ}\text{C}$, selected to represent experiments

248 conducted in aqueous solution or at the air-ice interface, respectively. For the air-ice interface
249 case, we used an ice slab model, with a well-equilibrated surface structure, in accordance with
250 recent measurements of the quasi-liquid layer of ice.^{43,44}

251 From each 50 ps-long MD simulation trajectory we extracted ~200 statistically independent
252 frames, removed the explicit solvent molecules, and computed the absorption spectra using
253 TDDFT.^{45,46} To account for the screening effect of the solvent, we used a self-consistent
254 continuous solvent (SCCS) model,^{47,48} with a position-dependent dielectric permittivity of the
255 environment. This newly developed feature allows one to treat molecules adsorbed at the
256 interface between regions with different dielectric response, such as the air-ice interface. The
257 ensemble average accounts for the configurational sampling at finite temperature in the specific
258 solvation environment.^{40,49}

259 To quantify the effect of the bathochromic shift on the molecular photodissociation rates, we
260 refined the line shape of the lowest energy absorption band using a simple machine learning
261 approach based on the least absolute shrinkage and selection operator (LASSO) regression
262 model.⁵⁰ We verified that the TDDFT datasets obtained for guaiacol in solution and at the air-ice
263 interface are suitable to train a single model, which we applied to 5000 frames from each FPMD
264 trajectory. The LASSO model allows us to attain a finer estimate of the low-energy tails of the
265 spectra, which is needed to calculate the rate of photon absorption for a given illumination
266 condition. Additional details about the computational procedures and parameters are provided in
267 Supplementary Information Section S2. The detailed implementation and validation of our multi-
268 scale multi-model approach to calculate the shifts of UV-visible absorption spectra at the air-ice
269 interface are described in depth in a separate manuscript.⁵¹

270 **3 Results and Discussion**

271 **3.1 Example illumination experiment**

272 Figure 1 shows a typical illumination experiment, with each point representing one snow-filled
273 beaker. Dark controls show slight loss of guaiacol, most likely explained by volatilization, with
274 a measured rate constant ($k'_{\text{GUA,dark}} \pm 1 \text{ SE}$) of $0.00076 \pm 0.00033 \text{ min}^{-1}$ ($R^2 = 0.57$). In the
275 illuminated samples, we see much more loss due to photodegradation, with a rate constant (j_{GUA}
276 $\pm 1 \text{ SE}$) of $0.0033 \pm 0.00032 \text{ s}^{-1}$ ($R^2 = 0.91$). Subtracting the dark loss from the light loss, and
277 then dividing by the measured $j_{2\text{NB}}$ value for this experimental day (0.0024 s^{-1}), gives a
278 normalized photodegradation rate ($j^*_{\text{GUA}} \pm 1 \text{ SE}$) of $1.0 \pm 0.19 \text{ min}^{-1}/\text{s}^{-1}$.

279 **3.2 GUA photodegradation rate constants for each sample preparation method**

280 As described in section 2.3, we illuminated our samples using two different light conditions.
281 Figure 2 presents the results for experiments conducted under Light Condition 1 (LC1), where
282 we unknowingly had significant a photon flux below 290 nm. We normalized the (dark-
283 corrected) measured rate constants to the measured $j_{2\text{NB}}$ value for each experimental day to
284 remove the impacts of differences in photon fluxes between different sample types. As shown in
285 Figure 2, guaiacol photodegradation in aqueous solution occurs slowly, but is measurable and
286 statistically greater than zero. Average normalized photodegradation rates constants (j^*_{GUA}) in
287 freezer frozen and liquid nitrogen (LN2) frozen samples are similar to each other, and
288 approximately 3 times faster than in aqueous solution. For the next condition, where guaiacol

1
2
3 289 was vapor-deposited to a water ice surface (“VD to ice surface”), the average j^*_{GUA} is faster than
4 290 in freezer frozen or liquid nitrogen frozen samples, but the data are highly variable and not
5 291 statistically different from zero, making it difficult to draw any conclusions. Finally, for
6 292 guaiacol vapor-deposited to nature-identical snow (“VD to snow”) the average j^*_{GUA} is similar to
7 293 that for the vapor-deposited to ice surface samples. However, the experimental reproducibility is
8 294 much better, and guaiacol in these samples clearly has a faster average j^*_{GUA} than either the
9 295 freezer frozen solution, liquid nitrogen frozen solution, or aqueous samples.

12 296 We used the Tukey-Kramer test for multiple comparisons ($P < 0.05$) to generate statistical
13 297 groupings having statistically indistinguishable mean j^*_{GUA} values, given by the letters A, B, and
14 298 C across the top of Figure 2. Because of its high variability, the average j^*_{GUA} for vapor-
15 299 deposited to ice surface samples is indistinguishable from that of any of the other sample
16 300 preparation method. Freezer frozen and liquid nitrogen frozen samples have means
17 301 indistinguishable from each other. Each of the remaining sample types has differing j^*_{GUA}
18 302 values, with aqueous the lowest and vapor-deposited to snow the highest. As listed in Table 1,
19 303 the ratio of j^*_{GUA} for the aqueous : freezer frozen solution : liquid nitrogen frozen solution :
20 304 vapor-deposited to snow results for LC1 is 1 : 2.6 : 3.3 : 17, with a typical propagated relative
21 305 standard deviation of roughly 50% for each ratio.

24 306 To the best of our knowledge, our results are the first use of nature-identical snow to study
25 307 photodegradation of a chemical at the air-ice interface. This technique has several clear
26 308 advantages over vapor deposition to an ice surface. First, the much higher specific surface area
27 309 reduces the likelihood of a test compound aggregating on the surface. Based on previous work
28 310 with nature-identical snow made in a similar machine,³⁸ our snow likely has a specific surface
29 311 area of around $600 \text{ cm}^2/\text{cm}^3$ (snow surface area/water volume). Assuming a single guaiacol
30 312 molecule occupies a square 6 \AA on a side and the molecules do not overlap, our maximum
31 313 guaiacol concentration ($9 \text{ }\mu\text{M}$) covers only 3% of the available snow surface. By contrast, the
32 314 maximum guaiacol concentration in our vapor-deposited to ice samples (also $9 \text{ }\mu\text{M}$) would be
33 315 approximately 60 molecules thick if distributed across a homogeneous ice surface in the
34 316 illumination beaker. Secondly, the nature-identical snow findings are more representative of
35 317 natural conditions, as most photodegradation taking place in snow-covered regions of the world
36 318 occurs in snowpacks, not on monolithic ice surfaces. Finally, our experimental results show
37 319 greater consistency on snow as opposed to ice surfaces, allowing more accurate determination of
38 320 rate constants, as illustrated by the 95% CI error bars in Figure 2.

42 321 After completing illumination experiments using LC1, we discovered that our illumination
43 322 system was passing significant amounts of light at wavelengths as low as 250 nm, whereas the
44 323 lowest wavelength in polar tropospheric sunlight is approximately 290 nm. To remedy this
45 324 problem and improve the experimental setup, we installed two additional optical filters in our
46 325 system, a 295 longpass and a 400 shortpass: we term this Light Condition 2 (LC2). To reduce
47 326 experimental variability and improve the statistical confidence of our results, we also tamped
48 327 down LC2 snow samples approximately 10 mm and illuminated them for at least 24 hours.
49 328 Figure 3 and Supplementary Figure S5 show the wavelength profiles for both LC1 and LC2, as
50 329 well as the modeled actinic flux for solar noon on the summer solstice at Summit, Greenland.
51 330 The 295 longpass filter significantly reduces wavelengths below 295 nm, while the 400 shortpass
52 331 filter cuts out wavelengths from approximately 400 to 525 nm, which are irrelevant for guaiacol
53 332 photodegradation but can heat and degrade frozen samples, particularly snow. Supplementary

333 Figure S6 shows transmittance measurements for the three optical filters, as well as some other
334 materials used in our experiments. While LC1 allowed considerable light emissions below 290
335 nm, LC2 does not, and is closer to the expected summer sunlight condition in a polar region such
336 as Summit.

337 Using the LC2 condition, we reran illumination experiments for all illumination conditions
338 except vapor-deposited to ice, with results shown in Figure 4 and Table 1. LC2 j^*_{GUA} values are
339 less than LC1 values because of two factors: first, there are fewer photons present at the
340 wavelengths where guaiacol absorbs most strongly (250-290 nm, Figure 3), so $j^*_{\text{GUA,exp}}$ is
341 considerably lower for LC2 and more similar to expected environmental values. Second, while
342 2NB absorbs more strongly at shorter wavelengths, it continues to absorb significant light up to
343 400 nm,²⁰ so measured j^*_{2NB} values are only slightly less for LC2 than LC1 (Supplementary
344 Tables S1 and S2). Despite being lower overall, j^*_{GUA} values show the same relationship to each
345 other under LC2 as LC1 (Table 1), with a ratio of aqueous : freezer frozen solution : liquid
346 nitrogen frozen solution : vapor-deposited to snow of 1 : 6.3 : 5.4 : 77, and a relative standard
347 deviation for each ratio of approximately 50%. Tukey-Kramer comparisons yield the same
348 statistical groupings for LC2 as for LC1, shown by the letters A, B, and C on Figure 4: average
349 j^*_{GUA} values for freezer frozen solution and liquid nitrogen frozen solution sample treatments are
350 statistically indistinguishable from each other, but statistically higher than aqueous, while the
351 average j^*_{GUA} value for guaiacol vapor deposited to snow is statistically higher than all other
352 treatments. LC2 results support the same conclusions as LC1, that guaiacol at the air-ice
353 interface has a considerably faster photodegradation rate constant than in aqueous solution and
354 LLRs, and a somewhat faster photodegradation rate constant in LLRs than in aqueous solution.
355 Interestingly, enhancement ratios relative to aqueous are higher for LC2 than LC1; because the
356 guaiacol absorbance curve overlaps the LC2 photon flux curve less than the LC1 curve (Figure
357 3), experiments conducted using LC2 conditions may be more sensitive to a bathochromic shift
358 in guaiacol absorbance, resulting in the higher ratios. The fact that the reactivity enhancement at
359 the interface depends on the wavelength distribution of the photon fluxes highlights the
360 importance of using good quality simulated sunlight in laboratory experiments.

361 While previous studies comparing photodegradation rate constants in aqueous solution, LLRs,
362 and at the air-ice interface did not test guaiacol, several reported similar results as ours here, with
363 rate constants somewhat faster in LLRs and considerably faster at the air-ice interface.¹¹⁻¹³
364 However, the magnitude of the enhancements we found at the air-ice interface are significantly
365 greater than have been reported before; while previous studies reported rate constant increases of
366 4- to 9-fold for organic compounds,¹¹⁻¹³ our results on ice range up to 77-fold. Taken together,
367 these results suggest the photochemical reactivity for guaiacol is decidedly different at the air-ice
368 interface, in LLRs, and in aqueous solution.

369 3.3 GUA photodegradation in samples with reduced dissolved oxygen

370 To confirm that guaiacol decay in our experiments is controlled by direct photochemistry and not
371 indirect reactions with oxidants photoformed by trace contaminants, we examined the impact of
372 removing dissolved oxygen for LC1 conditions. We were particularly concerned about oxidizing
373 triplet excited states ($^3\text{C}^*$), which react readily with guaiacol and other phenols⁵² and whose
374 concentrations are enhanced by a factor of roughly 100 in ice LLRs relative to solution.⁵³ In an
375 aqueous solution, dissolved oxygen is a major sink of $^3\text{C}^*$, so reducing the amount of O_2 should

376 greatly increase the triplet steady-state concentration, with a resulting increase in the guaiacol
377 degradation rate constant if $^3C^*$ were an important sink. We tested for this possibility by
378 bubbling nitrogen (99.998% purity) at a flow rate of 40 ml min⁻¹ through 2 ml of 1 μM guaiacol
379 aqueous solution in a 2-ml HPLC vial for 2 or 4 minutes, then capping with PTFE septum caps.
380 We illuminated some samples as aqueous solution, and others after freezing in a laboratory
381 freezer; both sample types were illuminated horizontally to avoid shading from the opaque caps.

382 As shown in Figure S7 and Table S3, deoxygenating made no statistically significant difference
383 in guaiacol photodegradation in aqueous solution, indicating that direct photodegradation is the
384 major sink. In frozen samples, the mean j^*_{GUA} is roughly 40% lower in ice made from
385 deoxygenated solution (compared to air-saturated solution), which is the opposite of what we
386 would expect if $^3C^*$ were a major oxidant for guaiacol, indicating that triplets are insignificant
387 oxidants. This small effect of deoxygenation suggests that trace oxygen-dependent oxidants
388 (e.g., hydroxyl radical) could contribute to guaiacol loss during our ice illumination experiments,
389 but indicates that the major sink for guaiacol in ice is direct photodegradation.

390 **3.4 Light absorbance of guaiacol in solution and on at the air-ice interface**

391 Our results in Figures 1 and 2 indicate that guaiacol photodegradation is significantly enhanced
392 in ice, and especially on ice, compared to in solution. To understand the contribution of changes
393 in guaiacol light absorption to this enhancement at the air-ice interface, we used multiscale
394 molecular modeling to determine absorption at the interface. Figure 3 shows the measured
395 absorption spectrum of guaiacol in solution (solid red line), along with measured photon fluxes
396 for our two experimental conditions and TUV modelled values for Summit, Greenland in
397 summer. The small overlap between the tail of the aqueous guaiacol absorption spectrum and the
398 edge of the photon flux curves suggests that a red shift of the absorption band for guaiacol at the
399 air-ice interface relative to aqueous solution would significantly enhance photodegradation.
400 Figure 3 displays the lowest energy absorption bands for guaiacol in solution (dashed red line)
401 and at the air-ice interface (dashed blue line), computed with our first-principles multiscale
402 approach, with line-shapes refined using statistical learning. The theoretical spectra are
403 normalized to the amplitude of the experimental absorption band. Considering that TDDFT tends
404 to systematically underestimate excitation energies,⁵⁴ the agreement between the theory and
405 experiment for guaiacol in solution is very good, as the difference between the measured and
406 calculated peak positions is less than about 0.1 eV. Given the systematic nature of this shift,⁴⁹
407 differences computed for the same molecule in different environments (e.g., in solution and at
408 the air-ice interface) are physically meaningful. Furthermore, the theoretical band is somewhat
409 narrower than the experimental one, as it misses the tail of higher energy excitations, which are
410 not taken into account in the machine-learning (ML) model. We used this ML model to refine
411 the long-wavelength tail of the spectra, as this region is crucial to estimate the overlap between
412 molar absorptivities and photon fluxes in different solvation conditions.

413 Supplementary Figure S9 shows that the ML model developed using the guaiacol molecule in
414 both environments has a training R^2 of 0.863 and a testing R^2 of 0.815, along with a training
415 mean absolute error (MAE) of 1.74 nm and a testing MAE of 1.99 nm. These statistical metrics
416 suggest it is within reasonable accuracy (i.e. $MAE \leq 2nm$) to use a single LASSO model, fitted
417 on the space of a subset of molecular coordinates, to interpolate through the excitation energies
418 of guaiacol both in aqueous solution and at the air-ice interface, and that the uncertainty of our

1
2
3 419 calculated absorbance shift is approximately ± 2 nm. Further, the possibility to accurately fit the
4 420 excitation energies to a single LASSO model indicates that the modeled bathochromic shift
5 421 results from conformational changes to the guaiacol molecule caused by the local solvation
6 422 environment (solution or air-ice interface), rather than dielectric differences in the solvation
7 423 environment itself.

8
9
10 424 As shown in Figure 3, our modeling finds that the absorption spectrum of guaiacol at the air-ice
11 425 interface undergoes two significant changes relative to that computed for guaiacol in solution: a
12 426 bathochromic shift of ~ 5 nm and a small (6%) increase in intensity. A statistical analysis of the
13 427 quantum-chemical excitation energies, computed from frames extracted from the FPMD
14 428 trajectories, reveals that the guaiacol configuration is different on the ice surface compared to in
15 429 solution, and indicates that the bathochromic shift (and intensity increase) is caused by such
16 430 differences in the geometry of guaiacol, a model of which is shown in Figure 5a with heavy
17 431 atoms and the OH group labeled from 1 to 10. Figure 5b shows the individual contribution of
18 432 each atom to the absorbance spectrum difference in terms of the absolute magnitude of the
19 433 weight parameters from the LASSO model ($|W_{\text{LASSO}}|$). This data shows that almost all of the
20 434 absorbance shift can be evenly attributed to conformational changes of the six carbons in the
21 435 guaiacol aromatic ring, with minor contributions from the other atoms. This in accordance with
22 436 electronic structure calculations that show that both the HOMO and the LUMO states are
23 437 localized on the phenyl group. The most important difference for the position of the lowest-
24 438 energy absorption band amounts to an average change in the C-C bond length in the phenyl ring,
25 439 i.e. the carbon atoms labeled 1-6 in Figure 5a. The average of these distributions, computed over
26 440 ~ 5000 frames of each FPMD trajectory, is shifted by approximately 0.012 \AA to longer distances
27 441 for guaiacol on ice than in aqueous solution (Figure 5c). While other factors (such as bond angle)
28 442 may also play a part, these results indicate geometric changes in the guaiacol aromatic ring are
29 443 the major factor responsible for the change in light absorption at the air-ice interface.

33 444 **3.5 Relative importance of changes in absorbance and quantum yields on photodegradation** 34 445 **rates**

35
36
37 446 Our guaiacol computational studies predict a bathochromic absorbance shift of approximately 5
38 447 nm on an ice surface relative to in aqueous solution, and a hyperchromic absorbance increase of
39 448 approximately 6% (Figure 3). To assess the impact of these changes on guaiacol
40 449 photodegradation rates, we first determined the rate constant for light absorbance in solution, i.e.,
41 450 the product of the molar absorptivity and photon flux (with some additional factors) at each
42 451 wavelength, summed over all wavelengths (equation S6). We did this for our two experimental
43 452 light conditions LC1 and LC2, as well as for the modeled summer Summit TUV actinic flux.⁵⁵
44 453 The area under each resulting curve gives the total rate constant of light absorption in solution
45 454 for each illumination condition (Figure S8). To determine the rate constant of light absorption at
46 455 the air-ice interface, we did the same procedure, but now with various changes (i.e., variable
47 456 shifts and a 6% increase in absorption) in the aqueous absorbance spectrum to mimic absorbance
48 457 on the ice surface. Assuming that the quantum yield for GUA loss is the same in solution and on
49 458 ice, the ratio of rates of light absorption (with and without the changes) is equal to the ratio of the
50 459 rate constants for guaiacol loss, i.e., $j^*_{\text{GUA,shifted}} / j^*_{\text{GUA,no shift}}$.

51
52
53
54 460 Figure 6 shows the impact of various red and blue shifts on the total rate constant of light
55 461 absorption and, therefore, predicted j^*_{GUA} values. Red-shifting the guaiacol absorbance spectrum
56
57
58
59
60

1
2
3 462 moves the absorbance to wavelengths where there are more photons (Figure 3), increasing the
4 463 rate constant of light absorption and the resulting rate constant for guaiacol photodegradation.
5 464 But for our laboratory light conditions the results are modest. For our best estimate of the red-
6 465 shifting (5 nm) and hyperchromic absorbance increase (6%) that occurs with guaiacol on ice, the
7 466 rate constant of light absorption relative to aqueous solution increases only by a factor of 1.5
8 467 (LC1) or 1.9 (LC2); incorporating our approximately 2-nm uncertainty in absorbance shift gives
9 468 ranges of 1.3 - 1.6 and 1.5 - 2.4 for LC1 and LC2 respectively. In contrast, we measured
10 469 photodegradation rate constant enhancements at the air-ice interface relative to aqueous solution
11 470 of 17- and 77-fold for LC1 and LC2, respectively (Table 1). So changes in light absorption only
12 471 explain a small portion (9% or less) of the observed enhancements in photodecay we measured
13 472 for guaiacol at the air-ice interface. As we have controlled for photon fluxes in our experimental
14 473 procedures, this suggests the remaining portion of the enhancement factors (11- to 13-fold for
15 474 LC1 and 32- to 51-fold for LC2) is caused by an increase in the quantum yield for guaiacol
16 475 photodegradation. In contrast to our laboratory photon flux results, the orange line in Figure 6
17 476 shows $j^*_{\text{GUA,shifted}} / j^*_{\text{GUA,no shift}}$ for various absorbance shifts using TUV-modeled actinic flux at
18 477 Summit, Greenland. Because there is only slight overlap (at around 300 nm) between this polar
19 478 actinic flux and the guaiacol absorbance curve (Figure 3), even small shifts in the absorbance
20 479 spectrum cause large changes in the amount of light absorbed. For example, including the 6%
21 480 absorbance increase and red-shifting the guaiacol spectrum by 1, 2, and 5 nm increases the rate
22 481 constant for guaiacol photodecay by factors of 1.7, 2.7, and 11 respectively relative to aqueous
23 482 solution, assuming no change in quantum yield.

24
25
26
27
28 483 Table 1 presents calculated quantum yields for guaiacol (Φ_{GUA}) under our various experimental
29 484 conditions. These are calculated using the aqueous guaiacol molar absorptivities for the solution,
30 485 freezer frozen solution, and liquid nitrogen frozen solution conditions; for values at the air-ice
31 486 interface (vapor-deposited to ice and vapor-deposited to snow), the calculations assume a 5-nm
32 487 bathochromic absorbance shift and 6% increase in molar absorptivities relative to solution.
33 488 Quantum yields are quite similar, nearly 3%, for aqueous solution in both LC1 and LC2
34 489 conditions. For preparations where guaiacol would largely be in LLRs (freezer frozen solution
35 490 and liquid nitrogen frozen solution), quantum yields are roughly 8% in LC1 and 17% in LC2, 3
36 491 and 6 times greater than in aqueous solution, respectively. Because we did not model
37 492 absorbance shifts in LLRs, it is possible that part of this apparent quantum yield increase could
38 493 be attributable to small (< 5 nm) absorbance shifts in LLRs. It is also possible that these sample
39 494 preparations place most of the guaiacol in LLRs, but also some at the air-ice interface, which
40 495 would increase the apparent quantum yield.

41
42
43
44 496 Finally, Table 1 shows that calculated quantum yields (± 1 SD) at the air-ice interface of snow
45 497 are very high – 31 (± 14) % for LC1 and 110 (± 50) % for LC2 – and are not statistically
46 498 significantly different from each other ($P < 0.05$). These represent enhancements by factors of
47 499 12 and 40 compared to aqueous for the LC1 and LC2 conditions, respectively. The calculated
48 500 quantum yield for LC2 snow encompasses the theoretical maximum of 1.0 mlc photon⁻¹, which
49 501 is exceptionally – and possibly erroneously – high. It is possible that other, unaccounted, factors
50 502 are contributing to this very high quantum yield. One possibility is that the true bathochromic
51 503 shift for guaiacol at the air-ice interface is greater than the 5 nm predicted by our computational
52 504 results, which would lower the calculated quantum yield. For example, a shift of 7 nm would
53 505 reduce the LC2 vapor-deposited to snow quantum yield to 0.89 mlc photon⁻¹. Another
54 506 possibility is that guaiacol is being lost via pathways other than direct photodegradation,

1
2
3 including through photoformed oxidants. Our deoxygenation control tests of Section 3.3 suggest
4 that oxidants are insignificant in aqueous solution but do play a role in guaiacol loss in ice. For
5 this reason our quantum yields should be considered upper bounds.
6

7 510 **4 Environmental implications and conclusions**

9
10 511 Guaiacol is one of the many aromatic compounds emitted by biomass burning,³⁹ which is a
11 512 significant source of organics to remote polar regions.⁵⁶⁻⁵⁹ To understand what our experimental
12 513 results mean for the lifetimes of guaiacol in polar snow, we calculated guaiacol photodegradation
13 514 rate constants for Summit, Greenland under summer solstice sunlight. We used equation 1 with:
14 515 TUV modeled actinic flux at midday of the summer solstice; our estimated average Φ_{GUA} under
15 516 LC2 for aqueous, LLRs (the average of freezer frozen solution and liquid nitrogen frozen
16 517 solution values) and at the air-ice interface (vapor-deposited to snow); and our measured ϵ_{GUA}
17 518 (bathochromically shifted by 5 nm and increased by 6% for guaiacol at the air-ice interface).
18 519 The resulting j_{GUA} values for Summit summer sunlight are 1.2×10^{-9} , 7.0×10^{-9} , and $5.2 \times 10^{-7} \text{ s}^{-1}$
19 520 for aqueous solution, LLRs, and the air-ice interface, respectively, corresponding to
20 521 photochemical lifetimes of 9,700, 1,600, and 22 days of midday summer solstice sunlight. In
21 522 comparison, based on the typical concentration of hydroxyl radical (OH) in Summit snow LLRs
22 523 ($2 \times 10^{-15} \text{ M}^{-1} \text{ s}^{-1}$; ⁶⁰) and the solution rate constant of OH with guaiacol (approximately 10^{10} M^{-1}
23 524 s^{-1} ; ⁶¹), the guaiacol lifetime with respect to OH oxidation in snow LLRs is roughly 14 hours. In
24 525 addition, triplet excited states of brown carbon are likely a similarly important sink for guaiacol,
25 526 as they react rapidly with phenols⁵² and their concentrations are enhanced in ice.⁵³ These results
26 527 indicate that while the photodecay of guaiacol at Summit is enhanced by a factor of roughly 100
27 528 at the air-ice interface compared to in LLRs, it is still relatively slow because of low light
28 529 absorbance. In contrast, reaction with photooxidants is a much more important sink for guaiacol,
29 530 rendering direct photoreaction unimportant. However, this is not a generalizable result, as the
30 531 relative importance of oxidants and direct photoreaction will depend on the identity of the
31 532 compound and its reactivity. In addition, it is also possible that rates of reaction of organics with
32 533 photooxidants such as OH vary between LLRs and the air-ice interface, but to the best of our
33 534 knowledge have not been studied.
34
35
36
37

38 535 As best we know, this work represents the first time that nature-identical snow has been used to
39 536 measure reaction rates at the air-ice interface. The major advantage of this approach is the very
40 537 high specific surface area of the snow, which better mimics environmental conditions, reduces
41 538 aggregation, and can provide more precise measurements than vapor deposition to an ice pellet.
42 539 The computational methods used here provide realistic absorbance curves and allow estimation
43 540 of absorbance shifts at the interface, which are difficult to measure. We found a statistically
44 541 significant increase in photon-flux-normalized guaiacol photodegradation rate constants relative
45 542 to aqueous solution for both LLRs and at the air-ice interface: the rate constant enhancement was
46 543 modest for LLRs, ranging from 3- to 6-fold depending on the illumination conditions, but was
47 544 larger at the air-ice interface, ranging from 10- to 77-fold. Computational modelling suggests
48 545 approximately 2 - 9% of the rate constant increase we measure in the laboratory is attributable to
49 546 a red-shift and increase of absorbance that occurs for guaiacol on the surface of ice compared to
50 547 solution. This leads us to conclude the measured rate constant enhancements are largely due to
51 548 increased quantum yields for guaiacol in frozen systems. The ratio of quantum yields for
52 549 aqueous : LLRs : air-ice interface is 1 : 3 : 12 for our initial light condition (LC1) and 1 : 6 : 40
53 550 for LC2. In contrast, our calculations indicate that a shift in absorbance will have a more
54
55
56
57
58
59
60

1
2
3 551 dramatic effect under polar sunlight; in the case of guaiacol on Summit snow, a 5-nm shift in
4 552 absorbance combined with a 6% increase in molar absorptivities causes a 11-fold increase in the
5 553 rate constant for light absorption, which is approximately equal to the factor of increase in
6 554 quantum yield that occurs at the interface compared to LLRs.

8
9 555 Our computational finding here that the average guaiacol aromatic carbon-carbon bond length is
10 556 approximately 1% longer on an ice surface than in aqueous solution, combined with the modeled
11 557 5 nm absorbance shift and 6% absorbance increase, suggests slight changes in atomic
12 558 arrangements can produce significant alterations in molecular properties. As discussed earlier,
13 559 previous work has shown faster photodegradation rate constants in LLRs or at the air-ice
14 560 interface for some compounds, but not for others. Similarly, some studies have reported
15 561 absorbance shifts (either red or blue) for compounds on ice surfaces, while others did not.
16 562 Collectively, these results suggest properties such as bond length, absorbance, or quantum yield
17 563 can be altered by the association between a molecule and an ice surface, but such changes are
18 564 difficult to predict and may be compound specific. Additional work to evaluate chemical
19 565 properties on ice surfaces, both experimental and computational, will be required to better
20 566 understand ice-chemical interactions.

23 567 **Conflicts of Interest**

24
25 568 There are no conflicts of interest to declare.

27 569 **Acknowledgments**

28
29
30 570 We thank the National Science Foundation for funding (CHE 1806210 and AGS-PRF 1524857)
31 571 and Rebecca Boulden and Raven Lyric for experimental assistance.
32
33
34
35
36
37
38
39
40
41
42
43
44
45
46
47
48
49
50
51
52
53
54
55
56
57
58
59
60

572 **Tables**

573

Table 1 Summary statistics for each experimental preparation method under Light Conditions 1 and 2^a

	Number of Experiments	$j^*_{\text{GUA}}{}^b$ ($\text{min}^{-1}/\text{s}^{-1}$)	Enhancement ^c ($j^*_{\text{GUA},i} / j^*_{\text{GUA},aq}$)	Quantum Yield (Φ_{GUA}) ^d (mlc photon^{-1})
LC1 (Light condition 1)				
Aqueous	6	0.075 ± 0.012	1	0.027 ± 0.0045
Freezer frozen solution	6	0.20 ± 0.082	2.6 ± 1.2	0.070 ± 0.030
Liquid nitrogen frozen solution	4	0.25 ± 0.040	3.3 ± 0.8	0.089 ± 0.015
Vapor-deposited to ice surface	4	0.71 ± 0.52	9.5 ± 7.1	0.17 ± 0.13
Vapor-deposited to snow	6	1.28 ± 0.57	17 ± 8	0.31 ± 0.14
LC2 (Light condition 2)				
Aqueous	3	0.0088 ± 0.0038	1	0.027 ± 0.012
Freezer frozen solution	3	0.056 ± 0.0063	6.3 ± 2.8	0.17 ± 0.021
Liquid nitrogen frozen solution	3	0.048 ± 0.0075	5.4 ± 2.5	0.15 ± 0.024
Vapor-deposited to ice surface	0		--- No experiments done ---	
Vapor-deposited to snow	4	0.68 ± 0.26	77 ± 44	1.1 ± 0.50

^a Samples were held at 5 °C (aqueous samples) or -10 °C (all other preparations).

^b Listed j^*_{GUA} values (photon-flux normalized photodegradation rate constants) are means \pm 1 standard deviation.

^c Enhancement factors are the ratio of the mean j^*_{GUA} value for each preparation method to the mean aqueous j^*_{GUA} value for that light condition, \pm the propagated standard deviation.

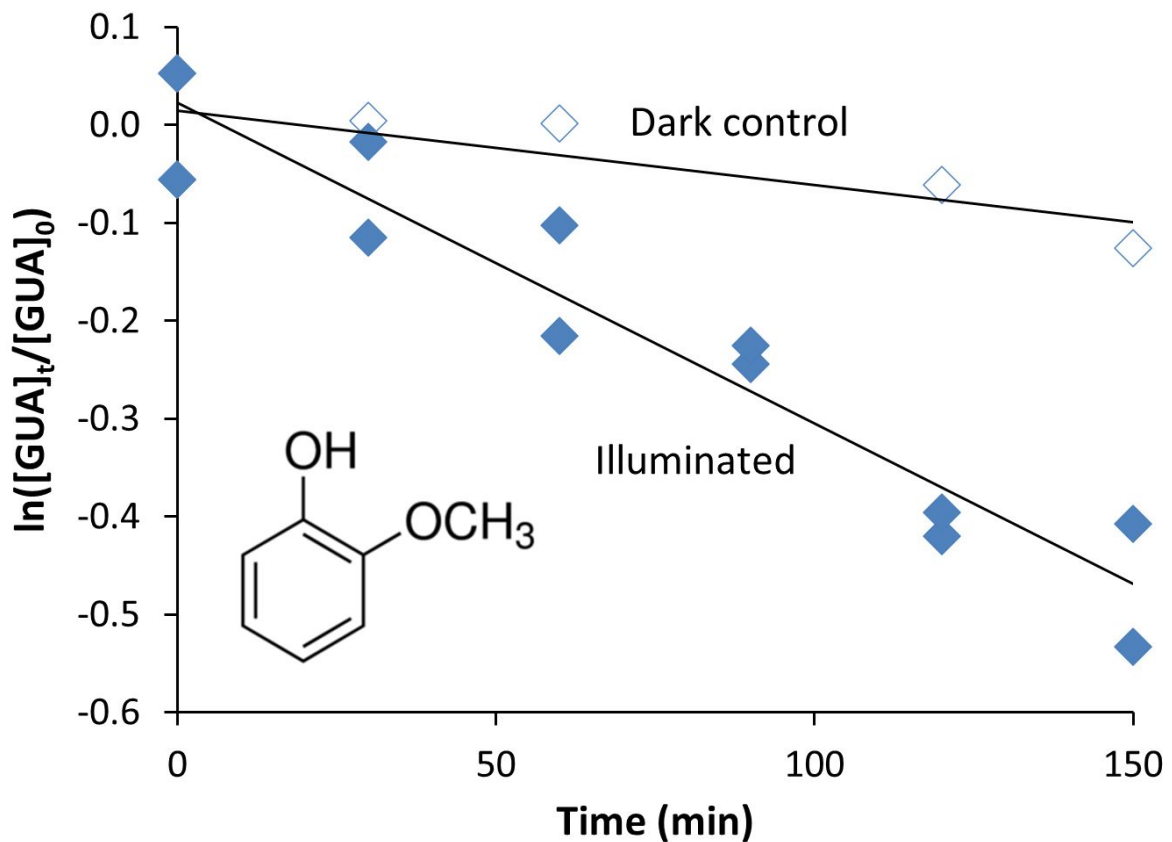
^d Quantum yields are calculated individually for each experiment from equation S7 in Supplementary Information Section S1, using the measured $j_{\text{GUA},\text{exp}}$ and $j_{2\text{NB}}$. Uncertainties for quantum yields are the propagated standard deviation for $j_{\text{GUA},\text{exp}}$ combined with the uncertainty for light absorption, assumed as 5% for aqueous, freezer frozen, and liquid nitrogen frozen sample types, or calculated from a 5 ± 2 nm absorbance shift for vapor-deposited samples (10% for LC1 or 25% for LC2 light conditions).

574

575

576

577

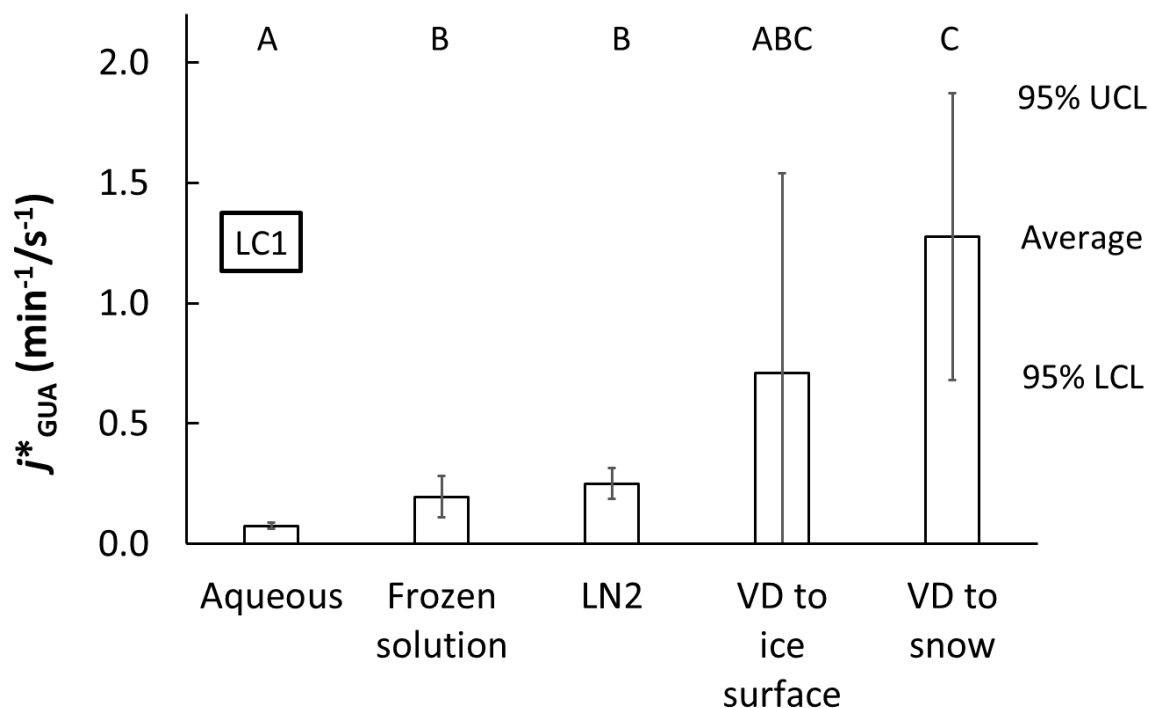
578 **Figures**

579

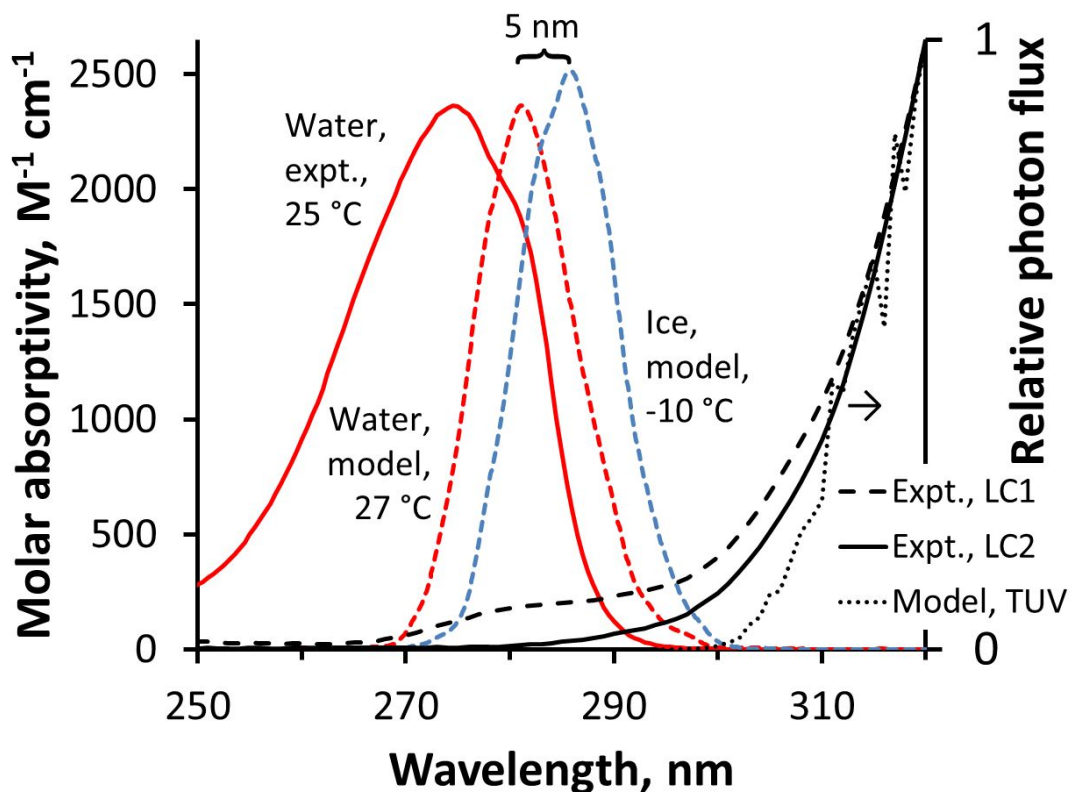
580 **Figure 1.** Loss of guaiacol (GUA) vapor-deposited to snow illuminated under Light Condition 1
581 (LC1) (blue diamonds) and in the dark (open diamonds). Each data point is from an individual
582 sample container; there are two separate illuminated samples at each time point. The value for
583 j_{2NB} (determined in aqueous solution and converted to the equivalent value in snow) is 0.0024 s^{-1}
584 and the initial guaiacol concentration (after melting) is $3 \mu\text{M}$.

585

586

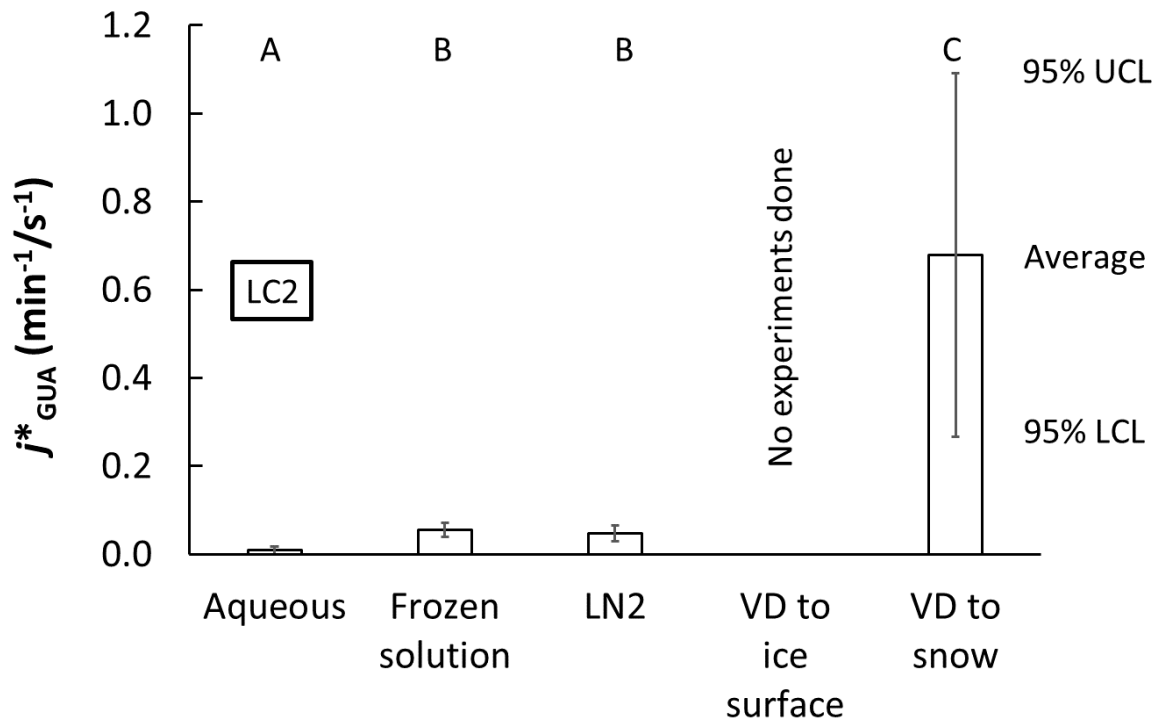


587
 588 **Figure 2.** Photon-flux-normalized photodegradation rate constants for guaiacol (j^*_{GUA}) under
 589 LC1 conditions for each sample preparation method: aqueous solution, solution frozen in
 590 laboratory freezer, solution frozen in liquid nitrogen (LN2), vapor-deposited to a water ice
 591 surface (“VD to ice surface”), and vapor-deposited to nature-identical snow (“VD to snow”).
 592 Samples were illuminated at 5 °C (aqueous samples) or -10 °C (all others). Bars indicate the
 593 mean value for each sample preparation method ($n = 4 - 6$), with 95% upper and lower
 594 confidence limits (UCL and LCL). Sample types having statistically indistinguishable average
 595 rate constants as determined by a Tukey-Kramer test ($P < 0.05$) are labeled with the same capital
 596 letter (“A”, “B”, or “C”); sample types with different letters have statistically different means.
 597
 598



599
600
601 **Figure 3.** Light absorption by guaiacol along with photon fluxes in our experiments and the
602 Arctic. Colored lines represent the measured molar absorptivities in aqueous solution (red line),
603 modeled aqueous absorbance (red dashed) and modeled absorbance on an ice surface (blue
604 dashed). The “5 nm” label represents the modeled bathochromic shift for absorbance on ice
605 versus in solution. Because the absorbance values of the modeled spectra are in arbitrary units,
606 the peak height of the modeled solution spectrum was fixed to equal the measured solution
607 spectrum and the modeled ice spectrum was adjusted by the same factor. Black lines (right axis)
608 show relative photon fluxes for the experimental LC1 and LC2 conditions, as well as for
609 Summit, Greenland at midday on the summer solstice from the TUV model. Photon fluxes are
610 relative and have been normalized to a value of unity at 320 nm.
611

612



613

614

615 **Figure 4.** Similar to Figure 2, but for LC2 light conditions. Photon flux-normalized
 616 photodegradation rate constants for guaiacol (j^*_{GUA}) for four sample preparation methods; vapor-
 617 deposited to ice surface (“VD to ice surface”) samples were not run for LC2. Bars indicate the
 618 mean value for each sample preparation method, with 95% upper and lower confidence limits
 619 (UCL and LCL). Sample types having statistically indistinguishable average rate constants are
 620 labeled with the same letter (“A”, “B”, or “C”).

621

622

623

624

625

626

627

628

629

630

631

632

633

634

635

636

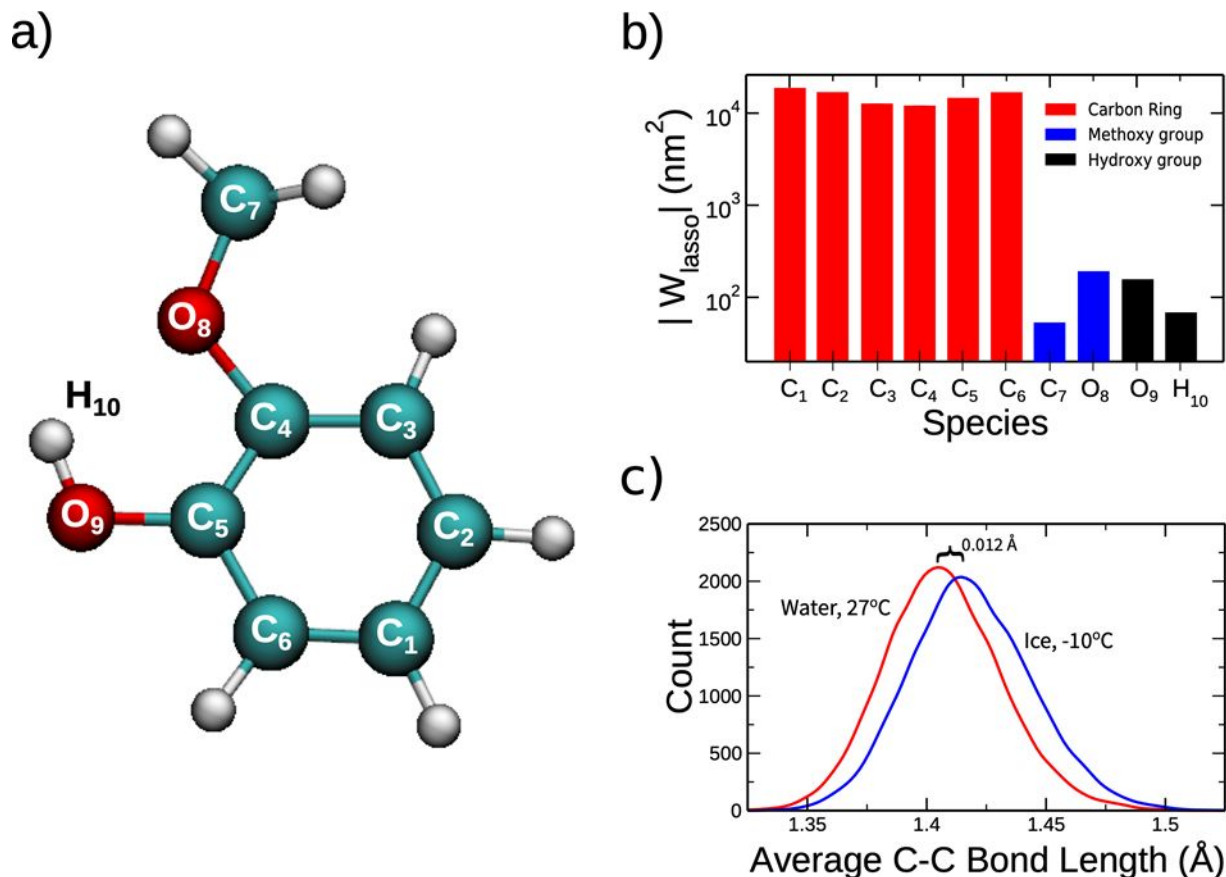
637

638

639

640

624



625

626

627

628

629

630

631

632

633

634

635

636

637

638

639

640

641

642

643

644

645

646

647

648

649

650

651

652

653

654

655

656

657

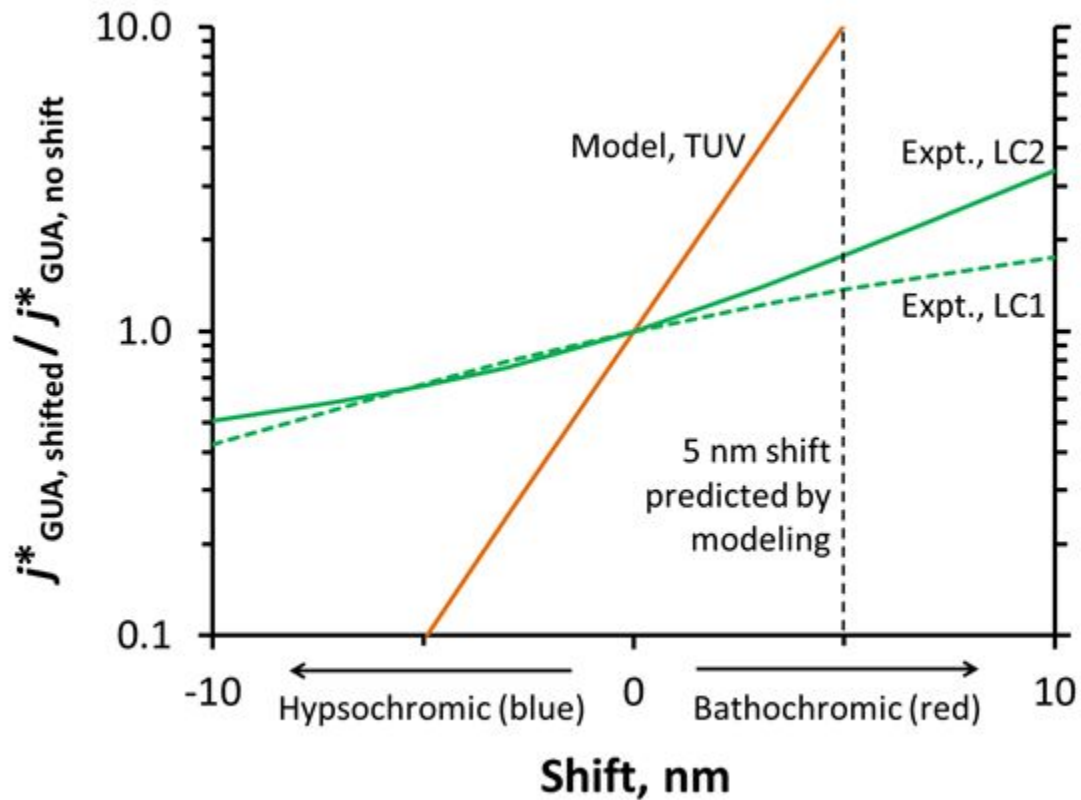
658

659

660

Figure 5. a) Diagram of a guaiacol molecule, showing atom labels. b) Results of LASSO analysis showing each atom's contribution to the modeled shift in absorbance spectrum at the air-ice interface. $|W_{\text{LASSO}}|$ is the absolute magnitude of the weight parameters from the LASSO model, expressed in nm². The aromatic ring carbons are the major contributors to the computed absorbance shift. c) Distribution of computed average carbon-carbon bond lengths for the guaiacol aromatic ring in solution (27 °C) and on the ice surface (-10 °C), showing a 0.012 Å increase in typical bond length on the ice surface. These results indicate a considerable change in guaiacol molecular conformation between the two different environments.

636



637

638 **Figure 6.** Predicted changes in j^*_{GUA} values resulting from various shifts in the guaiacol light
 639 absorbance spectrum relative to the aqueous (unshifted) spectrum. Hypsochromic (blue) shifts
 640 are represented by leftward movement on the X axis, while bathochromic (red) shifts are to the
 641 right. j^*_{GUA} values with a given shift were calculated using the TUV modeled actinic flux on the
 642 summer solstice for Summit, Greenland (orange line); measured flux for experimental condition
 643 LC1 (green dashed line); or measured flux for experimental condition LC2 (green solid line).
 644 The vertical dashed line shows the 5-nm bathochromic shift predicted for guaiacol by our
 645 molecular modeling.

646 **References**

- 647 1. T. Bartels-Rausch, H. W. Jacobi, T. F. Kahan, J. L. Thomas, E. S. Thomson, J. P. D.
648 Abbatt, M. Ammann, J. R. Blackford, H. Bluhm, C. Boxe, F. Domine, M. M. Frey, I.
649 Gladich, M. I. Guzman, D. Heger, T. Huthwelker, P. Klan, W. F. Kuhs, M. H. Kuo, S.
650 Maus, S. G. Moussa, V. F. McNeill, J. T. Newberg, J. B. C. Pettersson, M. Roeselova and
651 J. R. Sodeau, A review of air-ice chemical and physical interactions (AICI): liquids,
652 quasi-liquids, and solids in snow, *Atmos. Chem. Phys.*, 2014, **14**, 1587-1633.
- 653 2. F. Domine and P. B. Shepson, Air-snow interactions and atmospheric chemistry, *Science*,
654 2002, **297**, 1506-1510.
- 655 3. A. M. Grannas, A. E. Jones, J. Dibb, M. Ammann, C. Anastasio, H. J. Beine, M. Bergin,
656 J. Bottenheim, C. S. Boxe, G. Carver, G. Chen, J. H. Crawford, F. Domine, M. M. Frey,
657 M. I. Guzman, D. E. Heard, D. Helmig, M. R. Hoffmann, R. E. Honrath, L. G. Huey, M.
658 Hutterli, H. W. Jacobi, P. Klan, B. Lefer, J. McConnell, J. Plane, R. Sander, J. Savarino,
659 P. B. Shepson, W. R. Simpson, J. R. Sodeau, R. von Glasow, R. Weller, E. W. Wolff and
660 T. Zhu, An overview of snow photochemistry: evidence, mechanisms and impacts,
661 *Atmos. Chem. Phys.*, 2007, **7**, 4329-4373.
- 662 4. J. E. Dibb and M. Arsenault, Shouldn't snowpacks be sources of monocarboxylic acids?,
663 *Atmos. Environ.*, 2002, **36**, 2513-2522.
- 664 5. A. L. Sumner and P. B. Shepson, Snowpack production of formaldehyde and its effect on
665 the Arctic troposphere, *Nature*, 1999, **398**, 230-233.
- 666 6. M. Barret, F. Domine, S. Houdier, J. C. Gallet, P. Weibring, J. Walega, A. Fried and D.
667 Richter, Formaldehyde in the Alaskan Arctic snowpack: Partitioning and physical
668 processes involved in air-snow exchanges, *J. Geophys. Res.-Atmos.*, 2011, **116**.
- 669 7. H. W. Jacobi, R. C. Bales, R. E. Honrath, M. C. Peterson, J. E. Dibb, A. L. Swanson and
670 M. R. Albert, Reactive trace gases measured in the interstitial air of surface snow at
671 Summit, Greenland, *Atmos. Environ.*, 2004, **38**, 1687-1697.
- 672 8. G. J. Phillips and W. R. Simpson, Verification of snowpack radiation transfer models
673 using actinometry, *J. Geophys. Res.-Atmos.*, 2005, **110**.
- 674 9. E. S. Galbavy, C. Anastasio, B. L. Lefer and S. R. Hall, Light penetration in the
675 snowpack at Summit, Greenland: Part 1 Nitrite and hydrogen peroxide photolysis, *Atmos.*
676 *Environ.*, 2007, **41**, 5077-5090.
- 677 10. J. L. France, M. D. King, M. M. Frey, J. Erbland, G. Picard, S. Preunkert, A. MacArthur
678 and J. Savarino, Snow optical properties at Dome C (Concordia), Antarctica; implications
679 for snow emissions and snow chemistry of reactive nitrogen, *Atmos. Chem. Phys.*, 2011,
680 **11**, 9787-9801.
- 681 11. T. F. Kahan and D. J. Donaldson, Photolysis of polycyclic aromatic hydrocarbons on
682 water and ice surfaces, *J. Phys. Chem. A.*, 2007, **111**, 1277-1285.
- 683 12. T. F. Kahan, R. Zhao, K. B. Jumaa and D. J. Donaldson, Anthracene photolysis in
684 aqueous solution and ice: Photon flux dependence and comparison of kinetics in bulk ice
685 and at the air-ice interface, *Environ. Sci. Technol.*, 2010, **44**, 1302-1306.
- 686 13. T. F. Kahan, N. O. A. Kwamena and D. J. Donaldson, Different photolysis kinetics at the
687 surface of frozen freshwater vs. frozen salt solutions, *Atmos. Chem. Phys.*, 2010, **10**,
688 10917-10922.
- 689 14. L. Chu and C. Anastasio, Temperature and wavelength dependence of nitrite photolysis
690 in frozen and aqueous solutions, *Environ. Sci. Technol.*, 2007, **41**, 3626-3632.

- 1
2
3 691 15. L. Chu and C. Anastasio, Formation of hydroxyl radical from the photolysis of frozen
4 692 hydrogen peroxide, *J. Phys. Chem. A.*, 2005, **109**, 6264-6271.
- 5 693 16. L. Chu and C. Anastasio, Quantum yields of hydroxyl radical and nitrogen dioxide from
6 694 the photolysis of nitrate on ice, *J. Phys. Chem. A.*, 2003, **107**, 9594-9602.
- 7 695 17. K. Ram and C. Anastasio, Photochemistry of phenanthrene, pyrene, and fluoranthene in
8 696 ice and snow, *Atmos. Environ.*, 2009, **43**, 2252-2259.
- 9 697 18. T. Hullar, D. Magadia and C. Anastasio, Photodegradation Rate Constants for
10 698 Anthracene and Pyrene Are Similar in/on Ice and in Aqueous Solution, *Environ. Sci.*
11 699 *Technol.*, 2018, **52**, 12225-12234.
- 12 700 19. E. S. Galbavy, C. Anastasio, B. Lefer and S. Hall, Light penetration in the snowpack at
13 701 Summit, Greenland: Part 2 Nitrate photolysis, *Atmos. Environ.*, 2007, **41**, 5091-5100.
- 14 702 20. E. S. Galbavy, K. Ram and C. Anastasio, 2-Nitrobenzaldehyde as a chemical actinometer
15 703 for solution and ice photochemistry, *J. Photochem. Photobiol. A-Chem.*, 2010, **209**, 186-
16 704 192.
- 17 705 21. A. S. McFall and C. Anastasio, Photon flux dependence on solute environment in water
18 706 ices, *Environmental Chemistry*, 2016, **13**, 682-687.
- 19 707 22. C. Z. Zhu, B. Xiang, L. T. Chu and L. Zhu, 308 nm Photolysis of Nitric Acid in the Gas
20 708 Phase, on Aluminum Surfaces, and on Ice Films, *J. Phys. Chem. A.*, 2010, **114**, 2561-
21 709 2568.
- 22 710 23. A. S. McFall, K. C. Edwards and C. Anastasio, Nitrate Photochemistry at the Air-Ice
23 711 Interface and in Other Ice Reservoirs, *Environ. Sci. Technol.*, 2018, **52**, 5710-5717.
- 24 712 24. T. F. Kahan and D. J. Donaldson, Benzene photolysis on ice: Implications for the fate of
25 713 organic contaminants in the winter, *Environ. Sci. Technol.*, 2010, **44**, 3819-3824.
- 26 714 25. R. Kania, J. K. Malongwe, D. Nachtigallová, J. Krausko, I. Gladich, M. Roeselová, D.
27 715 Heger and P. Klán, Spectroscopic properties of benzene at the air-ice interface: A
28 716 combined experimental-computational approach, *J. Phys. Chem. A.*, 2014, **118**, 7535-
29 717 7547.
- 30 718 26. N. Matykiewiczová, R. Kurkova, J. Klanova and P. Klán, Photochemically induced
31 719 nitration and hydroxylation of organic aromatic compounds in the presence of nitrate or
32 720 nitrite in ice, *J. Photochem. Photobiol. A-Chem.*, 2007, **187**, 24-32.
- 33 721 27. D. Heger, J. Jirkovsky and P. Klán, Aggregation of methylene blue in frozen aqueous
34 722 solutions studied by absorption spectroscopy, *J. Phys. Chem. A.*, 2005, **109**, 6702-6709.
- 35 723 28. J. Krausko, J. K. Malongwe, G. Bičanová, P. Klán, D. Nachtigallová and D. Heger,
36 724 Spectroscopic properties of naphthalene on the surface of ice grains revisited: A
37 725 combined experimental computational approach, *J. Phys. Chem. A.*, 2015, **119**, 8565-
38 726 8578.
- 39 727 29. J. K. Malongwe, D. Nachtigallová, P. Corrochano and P. Klán, Spectroscopic properties
40 728 of anisole at the air-ice interface: A combined experimental-computational approach,
41 729 *Langmuir*, 2016, **32**, 5755-5764.
- 42 730 30. P. Corrochano, D. Nachtigallová and P. Klán, Photooxidation of Aniline Derivatives Can
43 731 Be Activated by Freezing Their Aqueous Solutions, *Environ. Sci. Technol.*, 2017, **51**,
44 732 13763-13770.
- 45 733 31. S. Gopalakrishnan, P. Jungwirth, D. J. Tobias and H. C. Allen, Air-Liquid Interfaces of
46 734 Aqueous Solutions Containing Ammonium and Sulfate: Spectroscopic and Molecular
47 735 Dynamics Studies, *J. Phys. Chem. B*, 2005, **109**, 8861-8872.
- 48
49
50
51
52
53
54
55
56
57
58
59
60

- 1
2
3 736 32. P. Jungwirth and D. J. Tobias, Specific Ion Effects at the Air/Water Interface, *Chem.*
4 737 *Rev.*, 2006, **106**, 1259–1281.
- 5 738 33. R. Vácha, L. Cwiklik, J. Řezáč, P. Hobza, P. Jungwirth, K. Valsaraj, S. Bahr and V.
6 739 Kempter, Adsorption of Aromatic Hydrocarbons and Ozone at Environmental Aqueous
7 740 Surfaces *J. Phys. Chem. A* 2008, **112**, 4942–4950.
- 8 741 34. R. B. Gerber, M. E. Varner, A. D. Hammerich, S. Riikonen, G. Murdachaew, D.
9 742 Shemesh and B. J. Finlayson-Pitts, Computational Studies of Atmospherically-Relevant
10 743 Chemical Reactions in Water Clusters and on Liquid Water and Ice Surfaces, *Accounts*
11 744 *Chem. Res.*, 2015, **48**, 399-406.
- 12 745 35. D. Heger, D. Nachtigallová, F. Surman, J. Krausko, B. Magyarova, M. Brumovsky, M.
13 746 Rubes, I. Gladich and P. Klán, Self-Organization of 1-Methylnaphthalene on the Surface
14 747 of Artificial Snow Grains: A Combined Experimental-Computational Approach, *J. Phys.*
15 748 *Chem. A.*, 2011, **115**, 11412-11422.
- 16 749 36. R. Kurkova, D. Ray, D. Nachtigallová and P. Klán, Chemistry of small organic molecules
17 750 on snow grains: The applicability of artificial snow for environmental studies, *Environ.*
18 751 *Sci. Technol.*, 2011, **45**, 3430-3436.
- 19 752 37. H. W. Jacobi, T. Annor and E. Quansah, Investigation of the photochemical
20 753 decomposition of nitrate, hydrogen peroxide, and formaldehyde in artificial snow, *J.*
21 754 *Photochem. Photobiol. A-Chem.*, 2006, **179**, 330-338.
- 22 755 38. S. Schlee, M. Jaggi, H. Lowe and M. Schneebeli, An improved machine to produce
23 756 nature-identical snow in the laboratory, *J. Glaciol.*, 2014, **60**, 94-102.
- 24 757 39. J. J. Schauer, M. J. Kleeman, G. R. Cass and B. R. T. Simoneit, Measurement of
25 758 emissions from air pollution sources. 3. C-1-C-29 organic compounds from fireplace
26 759 combustion of wood, *Environ. Sci. Technol.*, 2001, **35**, 1716-1728.
- 27 760 40. I. Timrov, M. Micciarelli, M. Rosa, A. Calzolari and S. Baroni, Multimodel Approach to
28 761 the Optical Properties of Molecular Dyes in Solution, *J. Chem. Theory Comput.*, 2016,
29 762 **12**, 4423-4429.
- 30 763 41. J. Bones and E. Adams, Davos, Switzerland, 2009.
- 31 764 42. H. Nakamura, A new apparatus to produce fresh snow, *Rep. Natl Res. Cent. Disaster*
32 765 *Prev.*, 1978, **19**, 229-237.
- 33 766 43. M. A. Sanchez, T. Kling, T. Ishiyama, M. J. van Zadel, P. J. Bisson, M. Mezger, M. N.
34 767 Jochum, J. D. Cyran, W. J. Smit, H. J. Bakker, M. J. Shultz, A. Morita, D. Donadio, Y.
35 768 Nagata, M. Bonn and E. H. G. Backus, Experimental and theoretical evidence for bilayer-
36 769 by-bilayer surface melting of crystalline ice, *Proc. Natl. Acad. Sci. U. S. A.*, 2017, **114**,
37 770 227-232.
- 38 771 44. T. Kling, F. Kling and D. Donadio, Structure and Dynamics of the Quasi-Liquid Layer at
39 772 the Surface of Ice from Molecular Simulations, *J. Phys. Chem. C*, 2018, **122**, 24780-
40 773 24787.
- 41 774 45. M. E. Casida, H. Chermette and D. Jacquemin, Time-dependent density-functional theory
42 775 for molecules and molecular solids Preface, *Theochem-J. Mol. Struct.*, 2009, **914**, 1-2.
- 43 776 46. D. Rocca, R. Gebauer, Y. Saad and S. Baroni, Turbo charging time-dependent density-
44 777 functional theory with Lanczos chains, *J. Chem. Phys.*, 2008, **128**, 14.
- 45 778 47. O. Andreussi, I. Dabo and N. Marzari, Revised self-consistent continuum solvation in
46 779 electronic-structure calculations, *J. Chem. Phys.*, 2012, **136**, 20.
- 47 780 48. O. Andreussi and N. Marzari, Electrostatics of solvated systems in periodic boundary
48 781 conditions, *Phys. Rev. B*, 2014, **90**, 16.
- 49
50
51
52
53
54
55
56
57
58
59
60

- 1
2
3 782 49. X. C. Ge, I. Timrov, S. Binnie, A. Biancardi, A. Calzolari and S. Baroni, Accurate and
4 783 Inexpensive Prediction of the Color Optical Properties of Anthocyanins in Solution, *J.*
5 784 *Phys. Chem. A.*, 2015, **119**, 3816-3822.
- 6 785 50. R. Tibshirani, Regression shrinkage and selection via the lasso: a retrospective, *J. R. Stat.*
7 786 *Soc. Ser. B-Stat. Methodol.*, 2011, **73**, 273-282.
- 8 787 51. F. Bononi, Bathochromic shift in the UV-Visible Absorption Spectra of Phenols at Ice
9 788 Surfaces: Insights from First-Principles Calculations, *In preparation*, 2020.
- 10 789 52. J. D. Smith, V. Sio, L. Yu, Q. Zhang and C. Anastasio, Secondary Organic Aerosol
11 790 Production from Aqueous Reactions of Atmospheric Phenols with an Organic Triplet
12 791 Excited State, *Environ. Sci. Technol.*, 2014, **48**, 1049-1057.
- 13 792 53. Z. Y. Chen and C. Anastasio, Concentrations of a triplet excited state are enhanced in
14 793 illuminated ice, *Environ. Sci.-Process Impacts*, 2017, **19**, 12-21.
- 15 794 54. M. Parac and S. Grimme, A TDDFT study of the lowest excitation energies of polycyclic
16 795 aromatic hydrocarbons, *Chem. Phys.*, 2003, **292**, 11-21.
- 17 796 55. S. Madronich and S. J. Flocke, in *Handbook of Environmental Chemistry*, ed. P. Boule,
18 797 Springer, Heidelberg, 1998, pp. 1-26.
- 19 798 56. J. R. McConnell, R. Edwards, G. L. Kok, M. G. Flanner, C. S. Zender, E. S. Saltzman, J.
20 799 R. Banta, D. R. Pasteris, M. M. Carter and J. D. W. Kahl, 20th-century industrial black
21 800 carbon emissions altered arctic climate forcing, *Science*, 2007, **317**, 1381-1384.
- 22 801 57. A. Pokhrel, K. Kawamura, B. Kunwar, K. Ono, A. Tsushima, O. Seki, S. Matoba and T.
23 802 Shiraiwa, Ice core records of levoglucosan and dehydroabietic and vanillic acids from
24 803 Aurora Peak in Alaska since the 1660s: a proxy signal of biomass-burning activities in
25 804 the North Pacific Rim, *Atmos. Chem. Phys.*, 2020, **20**, 597-612.
- 26 805 58. X. Wan, K. Kawamura, K. Ram, S. C. Kang, M. Loewen, S. P. Gao, G. M. Wu, P. Q. Fu,
27 806 Y. L. Zhang, H. Bhattarai and Z. Y. Cong, Aromatic acids as biomass-burning tracers in
28 807 atmospheric aerosols and ice cores: A review, *Environ. Pollut.*, 2019, **247**, 216-228.
- 29 808 59. G. T. Shi, X. C. Wang, Y. S. Li, R. Trengove, Z. Y. Hu, M. Mi, X. C. Li, J. H. Yu, B.
30 809 Hunter and T. H. He, Organic tracers from biomass burning in snow from the coast to the
31 810 ice sheet summit of East Antarctica, *Atmos. Environ.*, 2019, **201**, 231-241.
- 32 811 60. Z. Y. Chen, L. Chu, E. S. Galbavy, K. Ram and C. Anastasio, Hydroxyl radical in/on
33 812 illuminated polar snow: formation rates, lifetimes, and steady-state concentrations,
34 813 *Atmos. Chem. Phys.*, 2016, **16**, 9579-9590.
- 35 814 61. J. D. Smith, H. Kinney and C. Anastasio, Aqueous benzene-diols react with an organic
36 815 triplet excited state and hydroxyl radical to form secondary organic aerosol, *Phys. Chem.*
37 816 *Chem. Phys.*, 2015, **17**, 10227-10237.

817

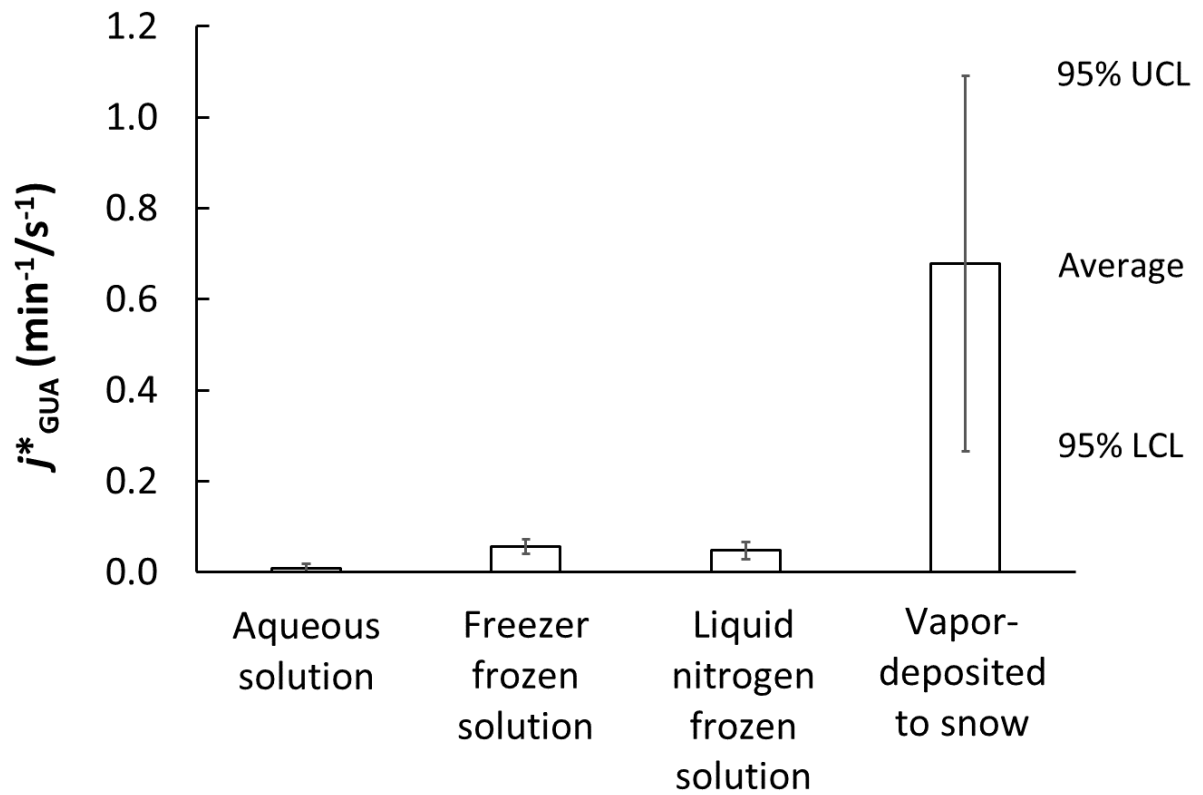


Table of contents figure. Guaiacol photodegradation rate constants in solution, liquid-like regions in ice (frozen solutions), and at the air-ice interface (vapor-deposited to snow).